inorganics

MDPI

Review

High-Pressure Routes to New Pyrochlores and Novel Magnetism

Haidong Zhou [1,2,†] and Christopher R. Wiebe [3,4,5,*,†]

1 Department of Physics and Astronomy, University of Tennessee, Knoxville, TN 37996-1200, USA; hzhou10@utk.edu
2 National High Magnetic Field Laboratory, Florida State University, Tallahassee, FL 32310-3706, USA
3 Department of Chemistry, University of Winnipeg, Winnipeg, MB R3B 2E2, Canada
4 Department of Chemistry, University of Manitoba, Winnipeg, MB R3T 2N9, Canada
5 Canadian Institute for Advanced Research, Toronto, ON M5G 1Z7, Canada
* Correspondence: chris.r.wiebe@gmail.com; Tel.: +1-204-786-9487
† These authors contributed equally to this work.

Received: 15 February 2019; Accepted: 26 March 2019; Published: 2 April 2019

Abstract: The pyrochlore structure ($A_2B_2O_7$) has been an object of consistent study by materials scientists largely due to the stability of the cubic lattice with respect to a wide variety of chemical species on the A or B sites. The criterion for stability under ambient conditions is controlled by the ratio of these cations, which is empirically $1.36 < R_A/R_B < 1.71$. However, under applied pressure synthesis conditions, the pyrochlore lattice is stable up to $R_A/R_B \sim 2.30$, opening up possibilities for new compounds. In this review, we will highlight recent work in exploring new rare-earth pyrochlores such as the germanates $RE_2Ge_2O_7$ and platinates $RE_2Pt_2O_7$. We highlight recent discoveries made in these pyrochlores such as highly correlated spin ice behavior, spin liquid ground states, and exotic magnetic ordering.

Keywords: geometrically frustrated magnetism; high-pressure synthesis; magnetic oxides

1. Introduction

The cubic pyrochlores of space group $Fd\bar{3}m$ have been known since 1826, discovered as a mineral family in Stavern, Norway [1]. The first species identified was $(Na, Ca)_2Nb_2O_6(OH, F)$, but the general chemical formula is $A_2B_2O_7$, where A and B are a variety of different cations [2]. From a solid-state chemistry perspective, the pyrochlore lattice is incredibly versatile allowing for a wide variety of chemical species upon the A or B sites [3]. The general stability criterion under ambient pressures is determined by the ratio of cation diameters $1.36 < R_A/R_B < 1.71$, where R_A and R_B are the A- and B-site crystal radii [4]. If the A and B sites have similar size, the fluorite phase is favored, which can be thought of as a disordered pyrochlore with random distributions of cations. If the A and B sites are too dissimilar in size, non-cubic phases are stable under atmospheric pressure conditions, such as the pyrogermanate phase [5]. Nonetheless, under ambient conditions, a plethora of stable cubic phases can be prepared, and for the titanates and stannates, nearly the entire rare-earth series can be prepared using standard solid-state methods [3]. The popularity of the titanate series in particular, with $RE_2Ti_2O_7$ (RE = rare-earth trivalent ion), in the condensed matter physics community is rooted in the relative ease of producing large single crystals using, for example, floating zone image furnaces. This provides a means of tuning the RE cation, and thus the f-electron magnetism on the A-site (with the B site being a stable diamagnetic Ti^{4+} state).

Upon further examination of the A-site magnetic sublattice, a network of corner-sharing tetrahedra is found. This connectivity of spins leads to a phenomenon known as geometric magnetic

frustration—the system has the possibility of not being able to satisfy all its local constraints simultaneously due to the lattice geometry. This can be illustrated most clearly in the two-dimension case of spins on an isolated triangle. For net antiferromagnetic interactions of spins that are constrained to lie up or down (or possessing Ising symmetry), the spins cannot satisfy a convention Néel antiferromagnetic ground state for nearest neighbors. Therefore, the system is said to be frustrated—the magnetic entropy cannot be released in forming a conventional ordered state. The new states which develop as energetic compromises, such as spin glasses (random freezing of spins), spin liquids (dynamic disordered spins at low temperatures), and spin ices, have been the objects of intense study over the last few decades. Spin ices, in particular—which are short-ranged ordered states of spins ordered over single tetrahedra in a 2-in, 2-out configuration—have been investigated as being host lattices for exotic magnetic excitations which are similar to magnetic monopoles. The delicate balance of conditions for producing these rare ground states (the magnitude of exchange interactions, crystal-field effects, and dipolar interactions) has led to a fervent search for new pyrochlore phases. Over the last decade, many solid-state chemists have turned towards high-pressure techniques to extend the chemical phase diagram of pyrochlores and find new examples of these phenomena (and even more surprising states of matter). This review article details this work, and speculates on the future of high-pressure pyrochlores that may be waiting on the horizon [4].

The evolution of high-pressure solid-state chemistry has progressed rapidly over the last few decades [4]. The "high-pressure" regime of solid-state chemistry is traditionally referring to applied pressures of over 0.1 GPa. One of the key advances was made by Walker in the 1990s to expand current methods much beyond his predecessors such as Bridgeman to bring applied pressures to over 10 GPa [6]. Walker-type presses are typically used for many of the preparations of the compounds within this review article, with yields on the order of milligrams per reaction. Pressures higher than 20 GPa and temperatures typically up to 2000 K can be obtained through diamond anvil cells, and high-pressure image furnace crystal growths are currently being pioneered by several research groups [7].

Many cubic pyrochlore phases have been synthesized under ambient pressure, as the tolerance factor determined by the ratio of cation diameters, $1.36 < R_A/R_B < 1.71$, where R_A and R_B are the A- and B-site crystal radii, enables a wide coverage of the periodic table (see Figure 1). For non-magnetic B-site cations such as Ti^{4+}, Zr^{4+} and Hf^{4+}, this has enabled the investigation of many chemical species without the use of high-pressure techniques. However, the issue of A/B-site mixing is relevant for R_A/R_B approaching unity, and there is also the issue of "stuffing" in species such as $Yb_2Ti_2O_7$ [8]. Some of these issues can be resolved using standard solid-state chemistry techniques, but higher quality single crystals could be obtained under applied pressure where the effects of mixing can be minimized, but not completely avoided. The issue of oxygen non-stoichiometry is also a factor which can highly affect the resultant magnetic ground state, as shown in such systems as $Tb_2Ti_2O_7$, which has radically different ordered states for changes in oxygen stoichiometry of less than 1 percent [9]. High-pressure techniques have, in general, even less control of the oxygen stoichiometry than reactions under ambient conditions. The long-term stability of phases produced under high pressure is also an issue, with changes in oxygen stoichiometry overtime leading to decomposition to more thermodynamically favored species such as the fluorite phases, or mixtures of fluorite and pyrochlore phases [10].

This review will focus on new high-pressure phases of RE pyrochlores. There are numerous studies of pyrochlores in the literature which have both A and B sites as being magnetic, [11] but for the purposes of this review we will only cover magnetism on one site. The various low-temperature magnetic phases of high-pressure pyrochlore phases can be divided into their spin symmetries: Ising, XY and Heisenberg.

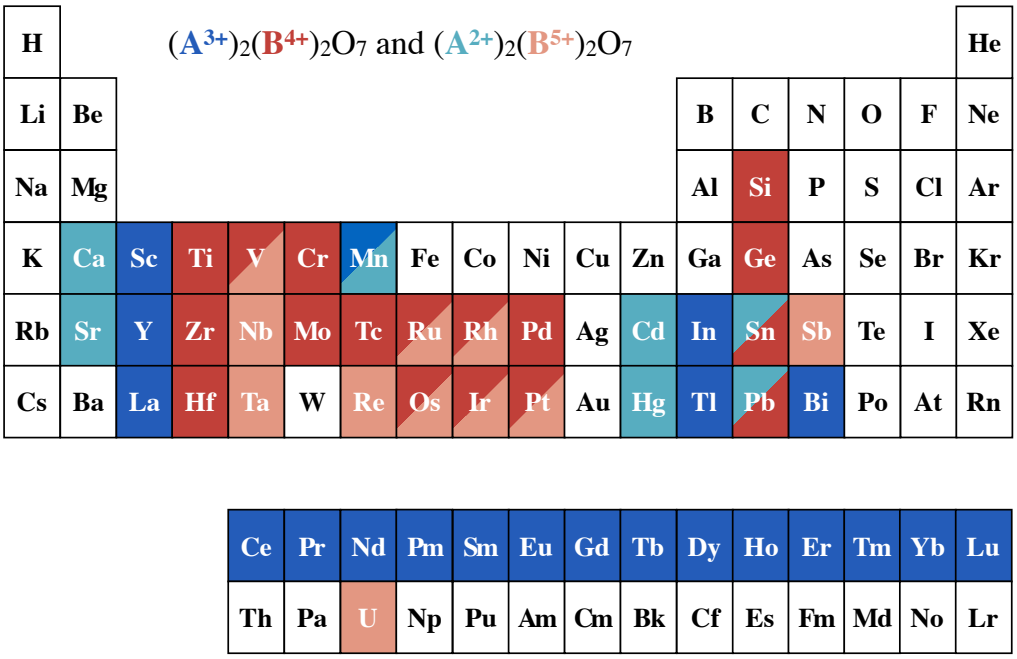

Figure 1. (color online) The periodic table with elements highlighted that can adopt the pyrochlore lattice. The colors indicate the elemental oxidation states, with 2+ in teal, 3+ in blue, 4+ in red, and 5+ in pink. Adapted from Ref. [4].

2. Heisenberg Spin Cases: $Gd_2Ge_2O_7$ and $Gd_2Pb_2O_7$

Gd^{3+} has seven unpaired f-electrons, and therefore the orbital angular momentum is quenched (L = 0) in a half-full shell and there is, as a result, an isotropic spin-only total angular momentum of S = J = 7/2. Crystal-field effects are not important, and the relevant physics of these ions follow the Heisenberg model with a ground state multiplet of 2J + 1 = 8 states. These are perhaps the simplest ground states to model and our review will begin with Gd high-pressure pyrochlore phases.

Li et al. [12] recently performed detailed studies on $Gd_2Ge_2O_7$ (GGO). As shown in Figure 2, at zero or small applied magnetic fields (H), the dc magnetic susceptibility (χ_{dc}), ac magnetic susceptibility χ_{dac}, and specific heat of GGO consistently show an anomaly or peak at T_N = 1.4 K, which represents a long-range magnetic ordering. For χ_{dc}, an extra shoulder around 0.9 K is induced with H = 1 T, which then shifts to below 0.6 K with H = 1.5 T. Meanwhile, χ_{ac} shows a more clear evolution of the field-induced anomalies: (i) at H = 1.5 T, a shoulder emerges around 0.9 K and then shifts to lower temperatures with increasing field; (ii) for H $>$ 1.5 T, the anomaly at 1.4 K splits into two peaks. The lower one shifts to lower temperatures and disappears while field increases to 3 T; (iii) for H $>$ 3 T, a new shoulder develops below 1.4 K and shifts to lower temperatures with increasing field; (iv) T_N is consistently suppressed by increasing field, which is also observed from specific heat. A magnetic phase diagram was constructed based on the data, as shown in Figure 3. At least four different magnetic phases can be distinguished here, which is similar to that of $Gd_2Sn_2O_7$ (GSO) [13,14].

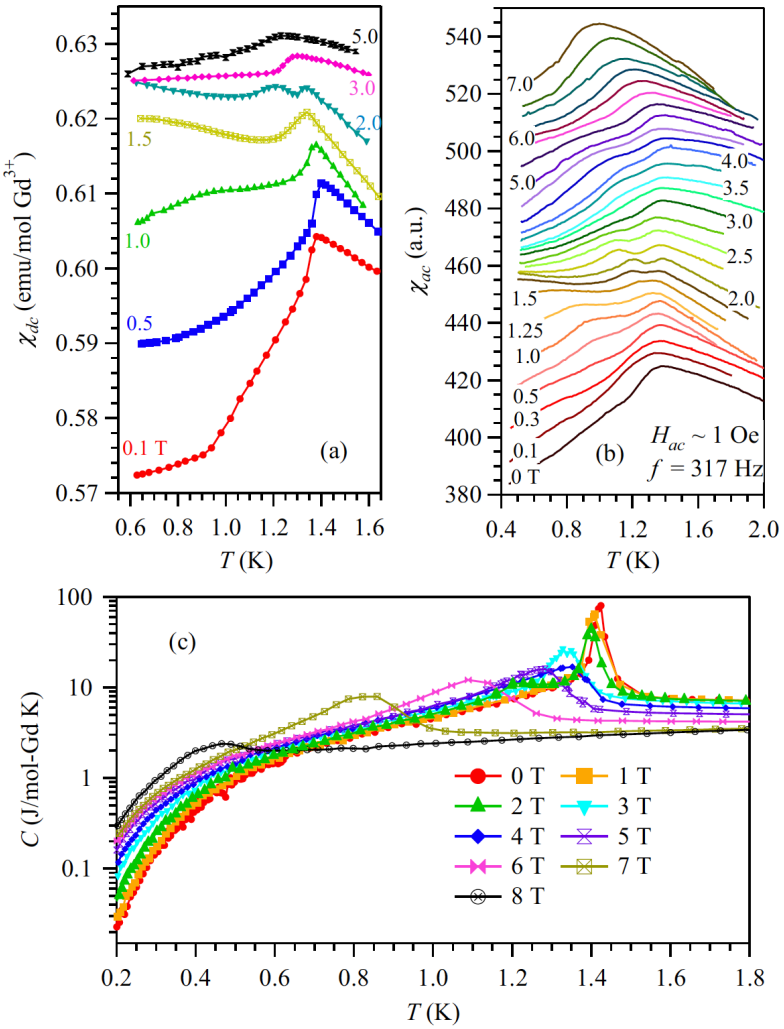

Figure 2. (color online) Temperature dependence of (**a**) dc magnetic susceptibility (χ_{dc}), (**b**) ac magnetic susceptibility χ_{ac}, and (**c**) specific heat (C) under various fields for $Gd_2Ge_2O_7$. From Ref. [12].

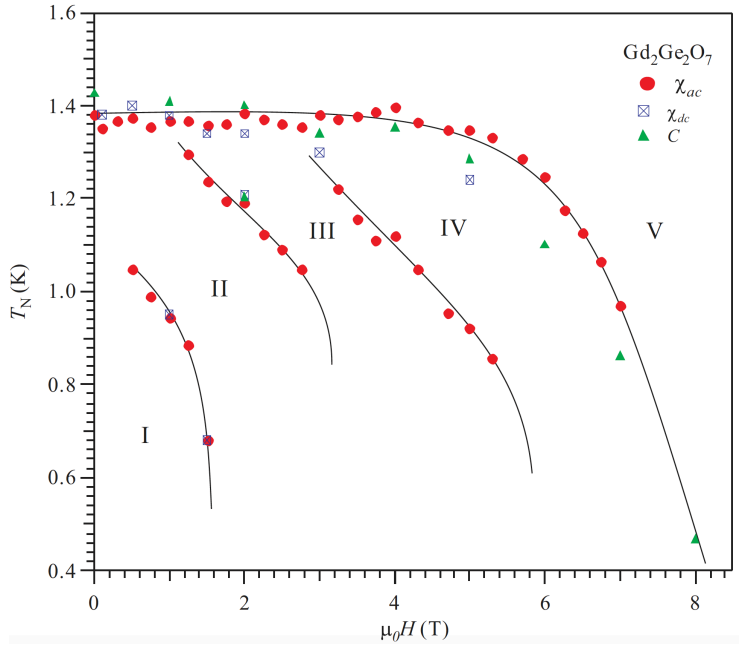

Figure 3. (color online) Magnetic phase diagram for $Gd_2Ge_2O_7$. From Ref. [12].

One of the interests in GSO originates from a magnetic transition at T_N = 1.0 K [15,16] with the magnetic structure exhibiting the so-called Palmer-Chalker (PC) state [17]. Meanwhile, $Gd_2Ti_2O_7$ (GTO) undergoes two transitions at T_{N1} = 1.0 K and T_{N1} = 0.75 K [18], while its exact magnetic structure is still under debate [19,20]. The T_N of GGO observed here is around 40% higher than those of GSO and GTO, which can be qualitatively attributed to the enhanced nearest-neighbor exchange interaction. This enhancement is naturally caused by the shorter nearest-neighbor Gd–Gd distance due to the smaller Ge^{4+} ionic size.

On the other side of the stability curve is the plumbate $Gd_2Pb_2O_7$. The first report of high-pressure synthesis of plumbate pyrochlores was made by Sleight in 1969 [21]. Pb^{4+} is the largest B-site cation that can be incorporated in the pyrochlore structure (r = 77.4 pm). However, the similarity in radii to the trivalent RE species leads to a considerable amount of chemical disorder. In the cases of $Nd_2Pb_2O_7$, the A/B-site disorder is on the order of a few percent, but in the case of $Gd_2Pt_2O_7$, the Gd site occupancy is 39%, which is nearly a completely disordered lattice [4,22]. Nonetheless, $Gd_2Pb_2O_7$ has a magnetic ordering transition at 0.81 K, and curiously a $T^{3/2}$ dependence of the heat capacity at low temperatures suggestive of ferromagnetic spin waves (Figure 4). This occurs despite the high degree of chemical disorder, and the large and negative Weiss constant of −7.38(6) K. This is in striking contrast to the magnetic ordering observed in $Gd_2Ti_2O_7$, which is a two-step process. The clear difference is the lack of chemical order in the plumbate, as both compounds have a lack of crystal fields and a large a negative Weiss temperature. Remarkably, the plumbate still orders into a well-defined magnetic ground state that is not a spin glass (even though the level of chemical disorder is beyond the percolation limit for the pyrochlore lattice). Future neutron scattering experiments with a less absorbing Gd isotope (such as Gd^{160}) are necessary to investigate this further.

3. Ising spin ices: $Ho_2Ge_2O_7$, $Dy_2Ge_2O_7$

Holmium and dysprosium pyrochlores are both examples of Ising-like systems where the spins are constrained to lie into or out of each tetrahedron at low temperatures due to strong crystal-field effects. Both magnetic species also have large moments on the order of 10 μ_B. Dipolar interactions are therefore very significant, but on an energy scale of ∼1 K. These conditions, with the additional constraint of net ferromagnetic interactions between the moments, lead to the so-called spin ice state: a short-range magnetic ordering of 2 spins pointing out of and two spins pointing into each tetrahedron at very low temperatures. The holmium and dysprosium pyrochlores have been studied extensively as host lattices for magnetic monopole excitations, which are spin defects of 3-in/1-out or 3-out/1-in spin states on each tetrahedron. Through a coarse-graining argument, these spin defects can be thought of as a source and sink of magnetic flux, and therefore as Dirac monopoles (Figure 5). The advantage to investigating high-pressure phases of these spin ices is to increase the monopole concentration through the application of chemical pressure (and therefore larger spin-spin interactions).

Hallas et al. studied $Ho_2Ge_2O_7$ (HGO) in detail to compare to the spin ice state of $Ho_2Ti_2O_7$ (HTO). As shown in Figure 6, the real part of the ac susceptibility, χ', of HGO drops at 1.3 K and approaches zero in the limit of 0.5 K while its imaginary part, χ'', contains a single maximum at 1.2 K. The frequency dependence of the peak position in χ'', T_1, can be fit to an Arrhenius law $f = f_0 \exp[-E_1/(k_B T_1)]$ with E_1/k_B = 20 K (Figure 6c). At high temperatures with a frequency of 1 kHz, a second peak begins to emerge in χ'' at 18 K with increasing applied filed (Figure 6d), which position (T_2) can be fit to the Arrhenius law with E_2/k_B = 196 K (Figure 6f).The presence and position of these peaks in the ac susceptibility for HGO is consistent with those for other known spin ices. The energy barrier of 20 K is related to local spins adopting an ice-like state. The comparable energy barriers for $Ho_2Sn_2O_7$ (HSO) and $Ho_2Ti_2O_7$ are 19.6 and 27.5 K, respectively [23]. The 196 K energy barrier of HGO relates to a thermally activated region and the first crystal-field excitation [24].

Zhou et al. studied the magnetic heat capacity (C_{mag}) of HGO (Figure 7a) [25]. The calculated zero-point entropy is near the characteristic spin ice zero-point entropy $S_0 = R \ln(3/2)$. The measured properties, including a small and positive Curie-Weiss constant, a magnetization saturating to half the

magnetic moment, and a magnetic diffusing scattering with pinch point singularities, are all evidence confirming that HGO is a dipolar spin ice. Similar behaviors were also observed for $Dy_2Ge_2O_7$ (DGO), which makes it another dipolar spin ice [25,26].

Zhou et al. [25] further studied the chemical pressure effects on studied spin ices by comparing their magnetic specific heat (Figure 8), including HSO, HTO, HGO, $Dy_2Sn_2O_7$ (DSO), $Dy_2Ti_2O_7$ (DTO), and DGO. According to the so-called "dipolar spin ice model" proposed by den Hertog and Gingras [27], the low-temperature magnetic properties of a pyrochlore spin ice are controlled by the magnetic exchange (J_{nn}) and dipolar interaction (D_{nn}) of the nearest-neighbor spins. The spin ice state is only stable with $J_{nn}/D_{nn} > -0.91$. For $J_{nn}/D_{nn} < -0.91$, the system undergoes a transition to a low-temperature Q = 0 antiferromagnetically ordered state. Moreover, the simulated specific heat using DSIM shows that its peak intensity and position is related to J_{nn}/D_{nn} ratio. With the experimental value of T_{peak} for specific heat and the calculated $D_{nn} = 5/3(\mu_0/4\pi)\mu^2/r_{nn}^3$ (where r_{nn} is the nearest-neighbor RE spin distance), the J_{nn}/D_{nn} values of all six spin ices were calculated and therefore located on the DSIM phase diagram. As shown in Figure 8, with increasing chemical pressure or decreasing lattice parameters, the Ge-spin ice approaches the phase boundary from the spin ice side. One noteworthy feature is that for DGO with smallest $J_{nn}/D_{nn} = -0.73$, its C_{mag} has the highest intensity, which is consistent with the sharp increase of C_{peak} calculated from DSIM as the spin ice system approaches $J_{nn}/D_{nn} < -0.5$ [28]. The possibility to stabilize a larger fraction of magnetic monopole in DGO also has been discussed by Zhou et al. in Ref. [26].

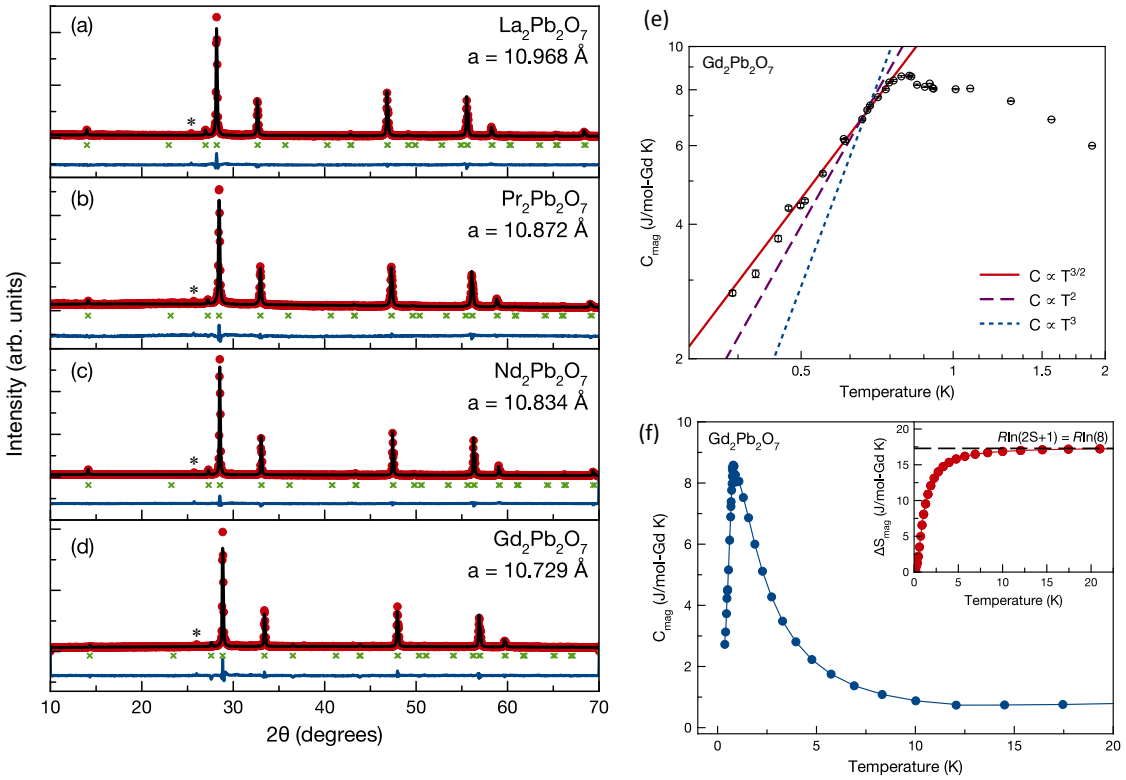

Figure 4. (color online) XRD patterns of (**a**) $La_2Pb_2O_7$, (**b**) $_2Pb_2O_7$, (**c**) $Nd_2Pb_2O_7$, and (**d**) $Gd_2Pb_2O_7$. The refinements are to the cubic pyrochlore structure (green crosses below the refinements) with the lattice parameter indicated for each. The asterix (black) marks the (111) Bragg reflection, which is weak due to chemical disorder. (**e**) Low-temperature heat capacity of $Gd_2Pb_2O_7$, showing a clear magnetic transition and a $T^{3/2}$ dependence suggestive of ferromagnetic ordering, despite the negative Weiss constant (**f**) Heat capacity and integrated entropy of $Gd_2Pb_2O_7$, indicating the release of the full S = 7/2 entropy with R ln(2S + 1) = R ln(8). From Ref. [22].

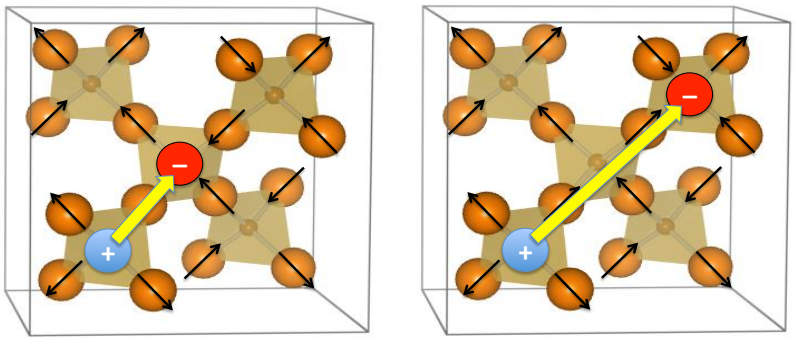

Figure 5. (color online) The creation and propagation of magnetic monopoles in dipolar spin ice. The 3-out, 1-in state is a source of magnetic flux (positive charge), and the 3-in, 1-out state is a sink of magnetic flux (negative charge).

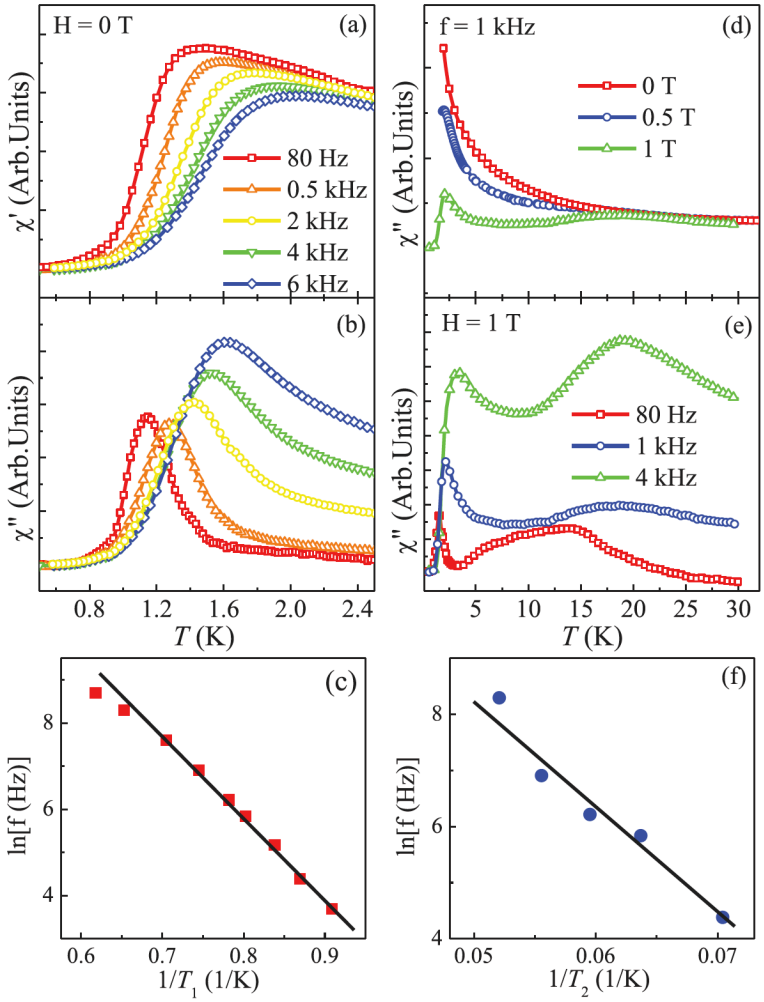

Figure 6. (color online)Temperature dependence of (**a**) the real part χ' and (**b**) the imaginary part χ'' of the ac susceptibility for $Ho_2Ge_2O_7$ below 3 K; (**c**) Arrhenius law fit of the low-temperature peak position in χ''; (**d**) high-temperature χ'' at f = 1 kHz with varying field strength; (**e**) high-temperature χ'' at H = 1.0 T with varying frequency; (**f**) Arrhenius law fit of the high-temperature peak position in χ''. From Ref. [29].

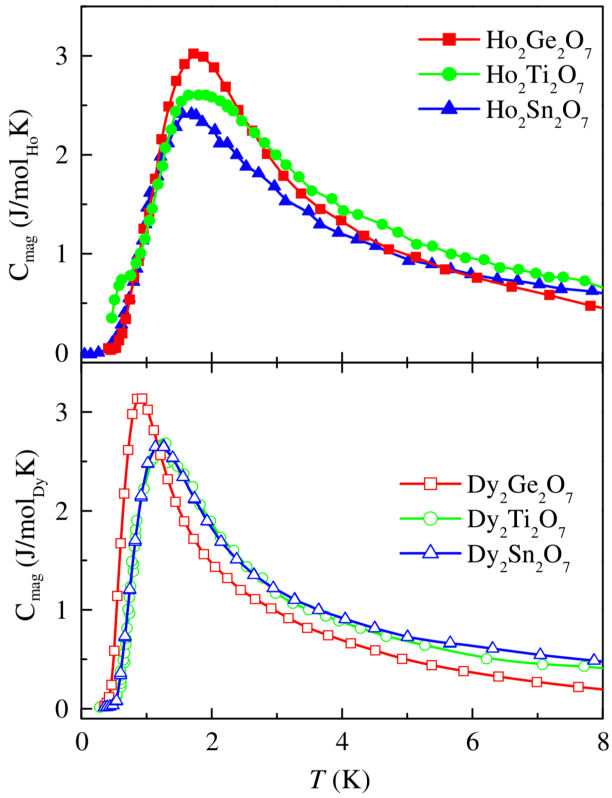

Figure 7. (color online) Magnetic specific heat for all six pyrochlore spin ices. The data for $Ho_2Sn_2O_7$ are from [30], $Ho_2Ti_2O_7$ from [31], and $Dy_2Ti_2O_7$ from [32]. From Ref. [25].

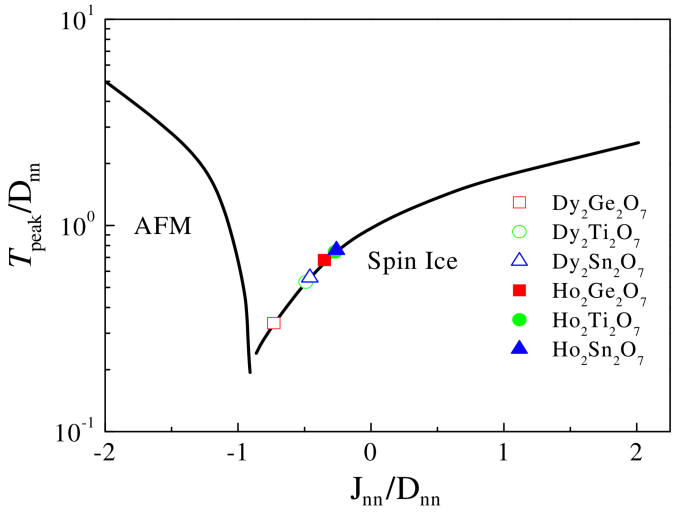

Figure 8. (color online) Dependencies of the specific heat peak position T_{peak}/D_{nn} on J_{nn}/D_{nn} ratio. The open symbols are experimental results, and the solid lines are the theoretical calculations from the dipolar spin ice model. From Ref. [25].

4. Ising Spin Liquid: $Tb_2Ge_2O_7$

$Tb_2Ti_2O_7$ remains one of the best examples in the literature as a candidate for a quantum spin liquid state. While the moment is much smaller than the holmium or dysprosium titanates, the spin-spin interactions are much stronger and dominantly antiferromagnetic in nature (with Weiss temperatures on the order of -17.5 K). The combination of these effects and low-lying crystal-field levels leads towards a dynamic ground state with antiferromagnetic ordering over single tetrahedra. To date there has been no evidence of long-range magnetic ordering down to mK temperatures.

The substitution of Ge^{4+} for Ti^{4+} results in even stronger exchange and therefore is a route to explore the fragility of spin liquids under chemical pressure.

Hallas et al. studied the magnetic properties of $Tb_2Ge_2O_7$ (TGO) [33]. A Curie-Weiss fit of the dc susceptibility leads a Weiss temperature $\theta_{CW} = -19.2$ K, representing net antiferromagnetic exchange interactions. The specific heat shows two anomalies around 5.5 K and 1.2 K. As shown in Figure 9, at zero dc field, both the χ' and χ'' show no sign of magnetic ordering down to 20 mK. An applied field as small as 0.01 T induces a broad peak in χ'. This peak is frequency independent (Figure 9c) but shifts to higher temperatures with increasing dc field. This field enhancement of this peak combined with its frequency independence suggest that the origin of this feature is ferromagnetic in character. Moreover, the increase of magnetic diffuse scattering intensity at low Q [33] also confirms the formation of ferromagnetic domains at low temperatures.

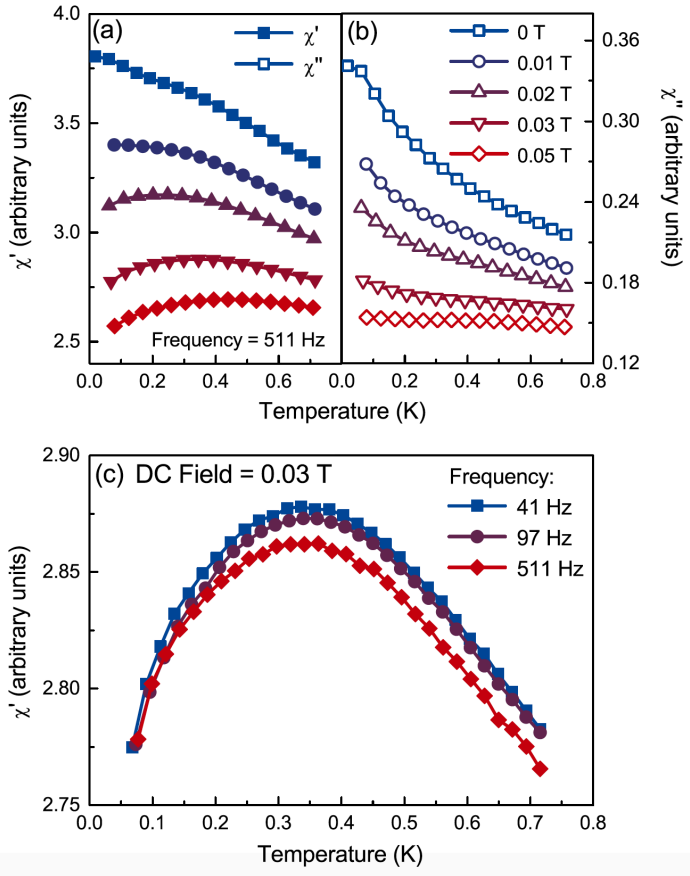

Figure 9. (color online) The (**a**) real, χ', and (**b**) imaginary, χ'', components of the ac susceptibility of $Tb_2Ge_2O_7$. (**c**) A dc field of 0.03 T induces a frequency independent peak that shifts to higher temperatures with increasing field. From Ref. [33].

From $Tb_2Ti_2O_7$ (TTO) to TGO, the decrease of lattice parameter leads to a 2% volume reduction. This reduction should increase the exchange interaction and therefore it is expected to see that TGO has a higher $\theta_{CW} = -19.2$ K than that of TTO ($\theta_{CW} = -17.5$ K [34]). The temperature dependence of the magnetic specific heat also appears to be similar [34]. Another similarity between them is that TTO also shows no ordering down to lowest temperature measured and have been treated as a quantum spin liquid candidate [35–39]. The surprising feature of TGO is that despite the enhanced antiferromagnetic (AFM) interactions, its ground state is ferromagnetic (FM) in nature. The chemical pressure here dramatically changes the magnetic ground state. This significant difference in the magnetism is possibly related to the subtle differences in the crystal-field scheme and, consequently, the single ion anisotropy between TGO and TTO due to chemical substitution, which needs further studies to clarify.

Very recent work by Hallas and Gaulin have shown that there is, indeed, a splayed ferromagnetic structure with T_C = 1.2 K [40].

5. XY Spin Case: $Er_2Ge_2O_7$/$Yb_2Ge_2O_7$

The XY pyrochlores, with planar local symmetry of the magnetic moments, have held the attention of the solid-state community due to the possibility of exotic magnetic states, such as the quantum spin ice. XY systems have also shown evidence for 2D magnetic ordering, and quasiparticle breakdown of spin wave spectra. There are several excellent reviews of these systems, including the recent review by Hallas, Gaudet and Gaulin [41].

As shown in Figure 10, Li et al. studied the ac susceptibility of $Er_2Ge_2O_7$ (EGO). At zero dc field and ambient pressure, χ' shows a maximum at T_N = 1.4 K, which is consistent with the peak position, or magnetic ordering, observed from the dc susceptibility and specific heat data [42]. With increasing dc field, χ' exhibits complicated behaviors: for H $\leq$ 0.2 T, T_N remains constant and χ' is enhanced below T_N; (ii) for 0.3 $\leq$ H $\leq$ 1.0 T, T_N decreases slightly and the low-temperature upturn of χ' is suppressed; (iii) for 1.0 $\leq$ H $\leq$ 2.3 T, the cusp-like anomaly of χ' becomes a broad peak, which shifts to lower temperatures with increasing fields; (iv) for 2.3 $<$ H $\leq$ 6.0 T, the feature of χ' is smeared out. The field dependence of χ' measured at 0.35 K (Figure 10e) again reflects this evolution. The χ'(H) data shows a double peak feature with the second peak at a critical field H_c = 2.3 T. The χ' data obtained under applied pressure also shows that both T_N and H_c are enhanced with increasing pressure (Figure 10f).

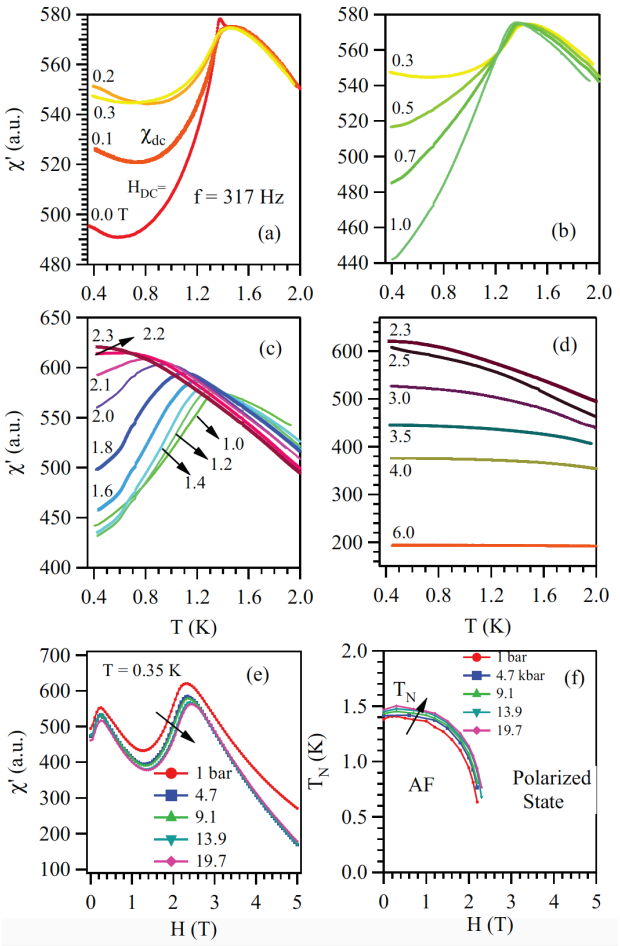

Figure 10. (color online) All data for $Er_2Ge_2O_7$. (**a**–**d**) Temperature dependence of the ambient-pressure χ' under different dc magnetic fields. (**e**) Field dependence of χ' measured at T = 0.35 K under different pressures. (**f**) Field dependence of T_N under different pressures. From Ref. [42].

Dun et al. measured the neutron powder diffraction of EGO under applied magnetic fields [43]. As shown in Figure 11, several magnetic Bragg peaks, such as (111), (220), and (311), are clearly observed at 0.3 K ($< T_N$ = 1.4 K). Moreover, the field dependence of the (220) and (311) Bragg peaks intensities shows complicated evolution: (i) with H $<$ 0.15 T, a magnetic domain alignment results in a quick drop of the (220) peak intensity with increasing field; (ii) between 0.15 and 2 T, the spins gradually rotate with the magnetic field but keep the AFM nature; (iii) around a critical field H_c = 2 T, the (220) Bragg peak intensity abruptly drops to a background value, while the (311) Bragg peak intensity continuously increases. This demonstrates that above H_c, EGO enters a spin polarized state. The observed FM(400) and AFM (200) Bragg peaks on the pattern measured at H = 5 T (Figure 11c) suggest that this polarized state is similar to the splayed ferromagnetic (SF) state in the Γ_9 manifold. This domain alignment around 0.15 T and the critical field around 2 T are consistent with the critical fields observed from ac susceptibility. The refinement of the 0.3 K data under zero field makes no difference between the Ψ_2 and Ψ_3 spin structure in the Γ_5 manifold. Meanwhile, the studies on $Er_2Ti_2O_7$ (ETO) [44,45] have shown that the applied field along the [1 −1 0] direction will select the two domains with lower intensity if the Ψ_3 phase is presented and lead to a drop of the (220) magnetic peak intensity with increasing field. Therefore, the drop of (220) peak intensity with applied field of EGO suggests a Ψ_3 ground state since the similar selection rule should also work in powder sample with additional averaging effect.

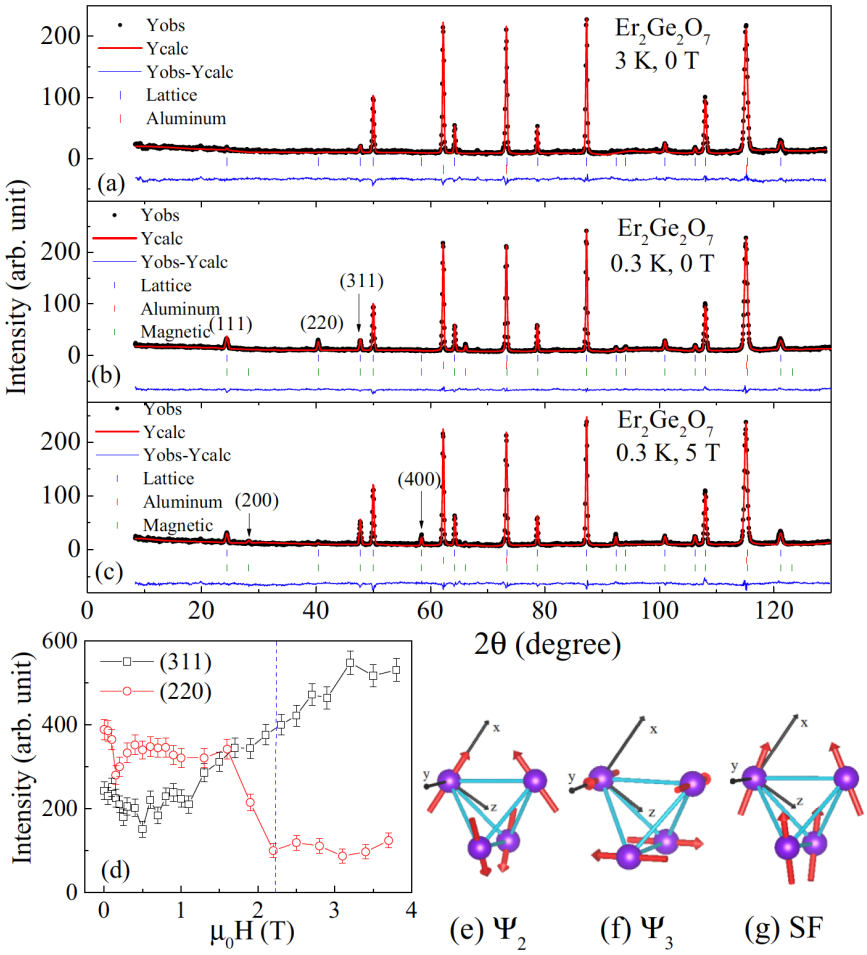

Figure 11. (color online) Elastic neutron scattering patterns and Rietveld refinements for EGO at (**a**) T = 3 K and H = 0 T, (**b**) T = 0.3 K and H = 0 T, and (**c**) T = 0.3 K and H = 5 T. (**d**) The field dependence of the (220) and (311) Bragg peaks intensities measured at T = 0.3 K; the critical field Hc is marked as the dashed line. The spin configurations for (**e**) Ψ_2, (**f**) Ψ_3, and (**g**) splayed ferromagnetic (SF) phases in the local coordination. From Ref. [43].

The ac susceptibility [46] and specific heat [43] measured by Dun et al. (Figure 12) confirm an AFM ordering at T_N = 0.62 K for $Yb_2Ge_2O_7$ (YGO). The observed magnetic Bragg peaks positions and intensity ratios from neutron powder diffraction measurements for YGO are very similar to those of EGO, which identifies YGO's ground state as either Ψ_2 or Ψ_3 state. Refinements based on these two spin structures give the same Yb^{3+} moment of 1.06 μ_B. The field dependence of the magnetic Bragg peak intensity (Figure 12c) and the ac susceptibility (Figure 11d) showing a double peak feature confirm that YGO undergoes a domain movement below 0.12 T and enters a SF (polarized) state above 0.22 T. YGO's phase diagram (Figure 12e) is similar to that of EGO but with lower T_N and smaller H_c. Later, another neutron study by Hallas et al. [47] leads to a smaller ordered moment, 0.3 μ_B/Yb ion. The exact reason for the difference of these two studies are still not clear. Their μSR measurements also indicate persistent weak spin dynamics below T_N.

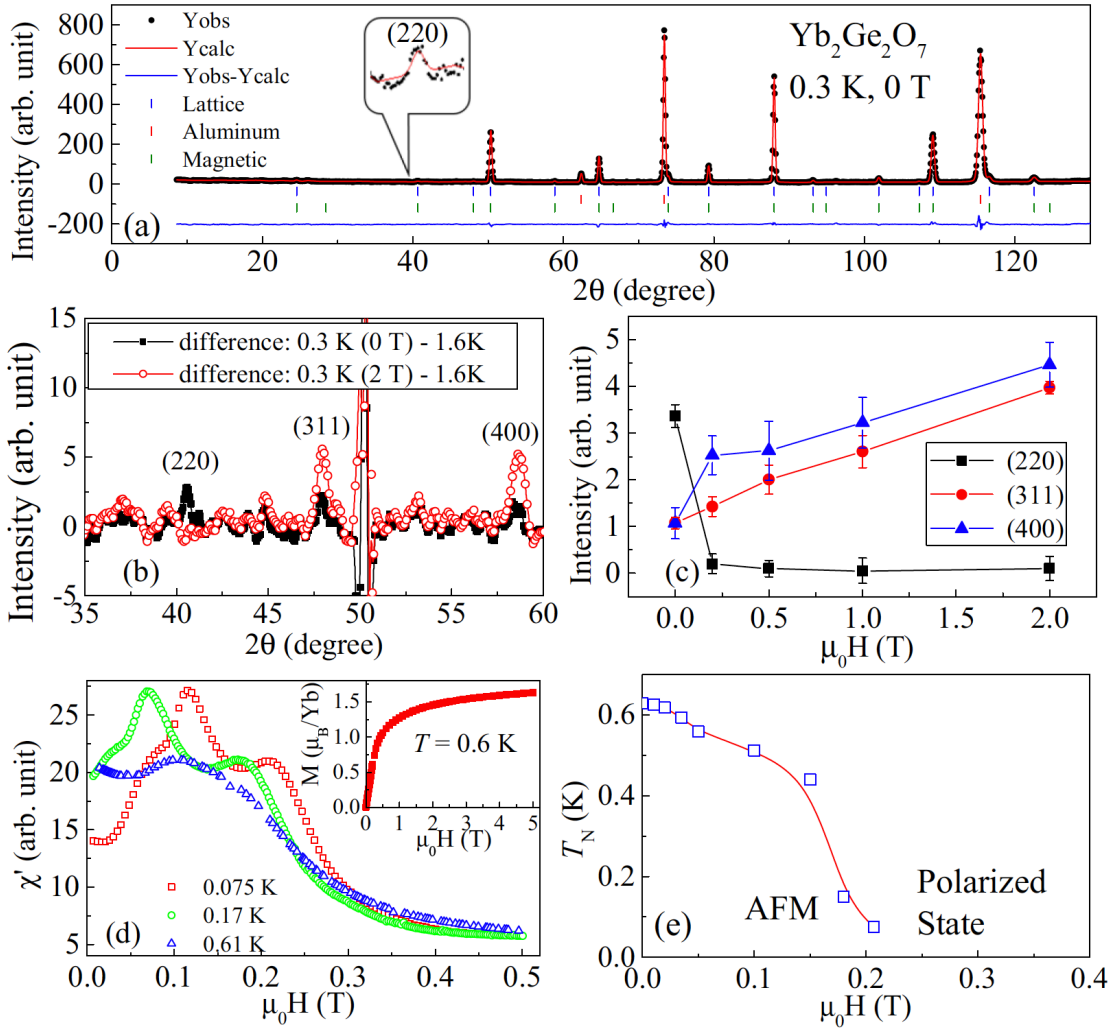

Figure 12. (color online) All data for $Yb_2Ge_2O_7$. (**a**) Elastic neutron scattering pattern and Rietveld refinement at T = 0.3 K and H = 0 T. (**b**) The difference between the patterns measured at 0.3 K (with H = 0 and 2 T) and 1.6 K. (**c**) The field dependence of the (220), (311), and (400) Bragg peaks intensities at 0.3 K. (**d**) The ac susceptibility at different temperatures. Inset: The dc magnetization measured at 0.6 K. (**e**) The magnetic phase diagram. From Ref. [43].

Table 1. Comparison between $Er_2X_2O_7$ and $Yb_2X_2O_7$.

	$Er_2X_2O_7$			$Yb_2X_2O_7$		
X site ion	Sn	Ti	Ge	Sn	Ti	Ge
IR(X^{4+})(Å)	0.69	0.605	0.53	0.69	0.605	0.53
a (Å)	10.35	10.07	9.88	10.28	10.03	9.83
θ_{CW}(K)	−14	−15.9	−21.9	0.53	0.75	0.9
T_N	0.1	1.17	1.41	0.15	0.24	0.62
Order type	∼(AFM)	AFM	AFM	FM	FM	AFM
Reference	[48,49]	[50]	[42]	[51]	[52]	[46]
Spin state	∼(PC)	ψ_2	ψ_3	SF	SF	$\psi_{2(or3)}$
Reference	[49]	[45]	[43]	[51]	[53]	[43]

Table 1 lists the properties of the studied XY pyrochlores, including $Er_2Sn_2O_7$ (ESO), ETO, EGO, $Yb_2Sn_2O_7$ (YSO), YTO, and YGO. With decreasing lattice parameters or increasing chemical pressure, (i) for Er-pyrochlores, the magnetic ground state changes from PC state for ESO, to Ψ_2 for ETO and then to Ψ_3 for EGO; (ii) for Yb-pyrochlores, it changes from ferromagnetic SF state for YSO and YTO to antiferromagnetic Ψ_2 or Ψ_3 state. It is very clear that the chemical pressure efficiently modifies the ground state of XY pyrochlores. A theoretical study [54] has pointed out that the anisotropic nearest-neighbor exchange interaction $J_{ex} = (J_{zz}, J_{\pm}, J_{z\pm}, J_{\pm\pm})$ between the R^{3+} ions, plus the strong quantum spin fluctuations of the effective spin-1/2 moment, stabilize various exotic magnetic ground states in these XY pyrochlores. Wong et al. [55] have scaled the J_{ex} by $J_{\pm}$ as three variables ($J_{zz}/J_{\pm}$, $J_{z\pm}/J_{\pm}$, $J_{\pm\pm}/J_{\pm}$) and calculated a two dimensional magnetic phase diagram with the fixed ratio of $J_{zz}/J_{\pm}$, which contains continuous phase boundaries among the PC, SF, ψ_2 and ψ_3 phases. Based on this phase diagram, the two trends for the Er- and Yb-pyrochlores' ground state change listed above can be successfully unified by the scenario that the increasing chemical pressure enhances $J_{\pm}$, which has been discussed in Ref. [43].

While the magnetic ground state, or the static properties, of the Yb-pyrochlores are distinct, the recent inelastic neutron scattering measurements [56] reported by Hallas et al. reveal a common character to their exotic spin dynamics. As shown in Figure 13, all three Yb-pyrochlores (YGO, YTO, and YSO) show a gapless continuum of spin excitations, resembling over-damped ferromagnetic spin waves at low Q. Furthermore, the specific heat of the series also follows a common form, with a broad, high-temperature anomaly followed by a sharp low-temperature anomaly at T_C or T_N. The spin dynamics observed from the neutron scattering measurements correlate strongly with the broad specific heat anomaly only, remaining unchanged across the sharp anomaly. These results suggest that the ordering in Yb-pyrochlores may not be simple magnetic dipole order, which needs future studies to clarify.

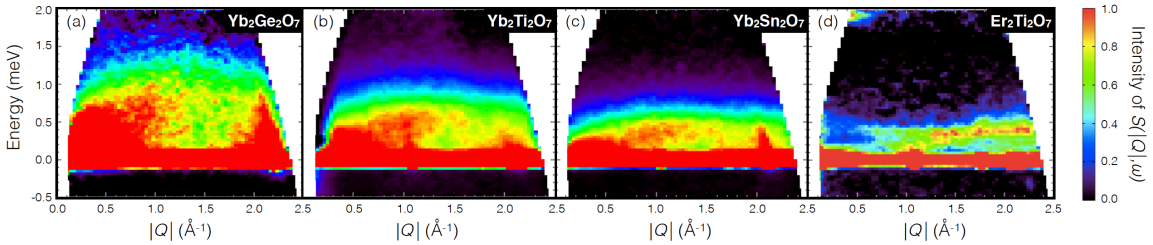

Figure 13. (color online) Inelastic neutron scattering spectrum for (**a**) YGO, (**b**) YTO, (**c**) YSO, and (**d**) ETO. From Ref. [56].

6. The Future of High-Pressure Pyrochlore Research: 4d and 5d Transition Metal Phases

The boundaries of the pyrochlore stability field discussed in this review are by no means set in stone. Ever more accessible higher pressures (greater than 20 GPa) and temperatures have led to new

phases, such as the recently discovered silicon pyrochlore phases (Si can have octahedral symmetry under high pressure) [57]. High-pressure techniques can also be used to stabilize certain oxidation states, such as Rh^{4+} and Pt^{4+} [58]. Here we highlight recent work on the planate pyrochlores.

Upon first glance, RE planate pyrochlores appear to be stable under ambient pressure, since the A/B ionic radius ratio is approximately 1.7. However, PtO_2 decomposes at around 450 degrees C, rendering standard solid-state synthesis methods infeasible. RE platinate pyrochlores can be synthesized in single phase form at relatively low pressures (6 GPa) and 1000 degrees C. The magnetic properties of many of these pyrochlores are quite different than their titanate analogues, even though Pt^{4+} is a d^6 system and should be diamagnetic in a filled t_{2g} orbital. $Gd_2Pt_2O_7$, for example, has an only 0.7 percent different lattice parameter than $Gd_2Ti_2O_7$. The ordering transition in $Gd_2Pt_2O_7$ occurs at T_N = 1.6 K, which is at least 50% higher than other Gadolinium-based pyrochlores which order at 1 K or lower (Figure 14) [59]. The reason for this is the enhanced magnetic exchange from the filled t_{2g} orbital for Pt^{4+}, which appears to remove the frustration. $Er_2Pt_2O_7$ represents another intriguing case where the apparent magnetic transition temperature decreases rather than increases when compared to the titanate analogue (T_N = 0.35 K for $Er_2Pt_2O_7$ compared to T_N = 1.1 K for $Er_2Ti_2O_7$) [60]. Again, structurally the two compounds only have a 0.5 percent lattice constant difference. The reason for this decrease in T_N is linked to the proximity to a competing magnetic phase. $Er_2Pt_2O_7$ magnetically orders into the Palmer-Chalker magnetic structure (Γ_7) but the exchange interactions place the system very close to the Γ_5 phase. Enhanced spin fluctuations close to the spin boundary are seen on the order of T = 1 K through inelastic neutron scattering measurements [60].

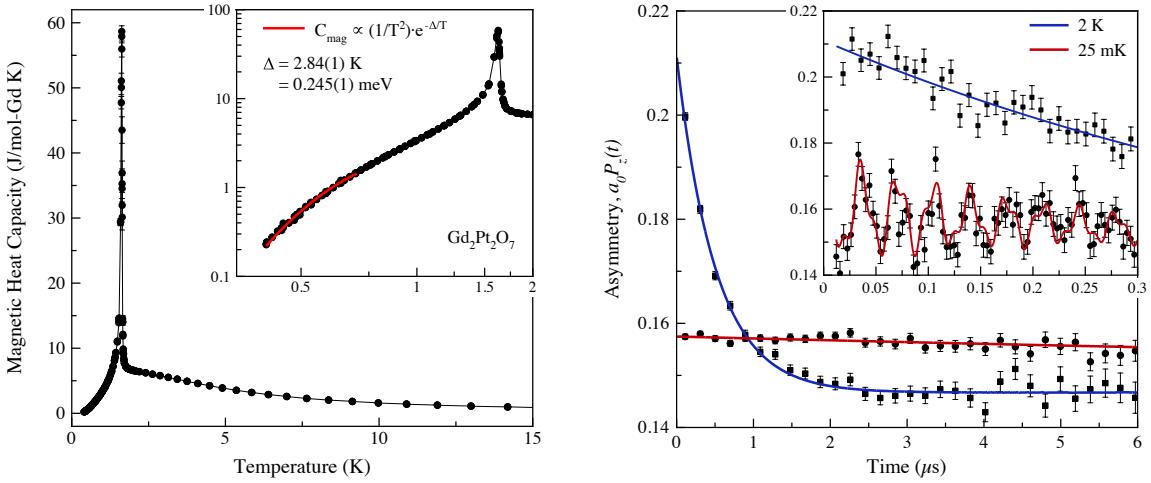

Figure 14. (color online) Heat capacity (left) and muon spin relaxation measurements (right) on $Gd_2Pt_2O_7$, showing clear evidence for long-range magnetic ordering. From Ref. [59].

7. Conclusions

The future of high-pressure pyrochlore synthesis likely involves further extensions of the stability field (through higher pressures greater than 20 GPa), and the stabilization of delicate oxidation states as mentioned above. The exploration of magnetic species on both the A and B sites is also promising, as exotic magnetic behavior, such as the giant magnetoelectric effect in $Er_2Mn_2O_7$, can be observed [61]. The importance of high pressure as a vector for materials discovery is all the more apparent with the plethora of pyrochlore phases mentioned above, and as well the new advances in other geometrically frustrated magnets, [62] and the discovery of near room temperature superconductivity in hydrides [63]. The discovery of the latter in particular has brought high-pressure research, again, to the forefront of the condensed matter physics community. As many of these new phases of matter are only metastable at high pressures, there will also be a further impetus to develop fast, in situ, characterization techniques in this regime. X-ray and neutron scattering probes at powerful, high brightness sources will be essential for moving this field forward. As well, it is clear that the boundaries of the stability field of

pyrochlore oxides synthesized under high pressure are destined to change rapidly as new materials will become accessible. The silicate RE pyrochlores are of great interest as this provides a mechanism to, for example, study high density monopole phases in species such as $Dy_2Si_2O_7$ [57]. Mixed pyrochlore phases of the form RE_2ScNbO_7, which are only stable under ambient conditions to Dy in the RE series, could also be stabilized under moderate high pressures on the other side of the stability field. This enables unique studies of B-site chemical disorder, and the possibility of Nb^{5+}/Sc^{3+} charge ice phases forming. The role of local disorder on the B sites will require techniques such as pair distribution function analysis, which is another rapidly developing technique in the study of solids [64]. It is clear that the use of high-pressure solid-state chemistry methods to explore new materials is still in its infancy and has ample room for growth in the near future.

Author Contributions: H.Z. and C.R.W. contributed equally to the writing of this review article.

Funding: This research was funded in part by the National Science and Engineering Research Council of Canada (NSERC), and the Canadian Foundation for Innovation (CFI). C.R.W. would like to thank the Canadian Institution For Advanced Research (CIFAR) and the Canada Research Chair program (Tier II). H.Z. would like to thank the support from the NSF-DMR through Award DMR-1350002.

Conflicts of Interest: The authors declare no conflict of interest.

References

1. Subramanian, M.A.; Aravamudan, G.; Rao, G.V.S. Oxide Pyrochlores: A Review. *Prog. Solid State Chem.* **1983**, *15*, 55–143. [CrossRef]
2. Barthelmy, D. Pyrochlore Mineral Data. Available online: webmineral.com (accessed on 3 February 2015).
3. Gardner, J.S.; Gingras, M.J.P.; Greedan, J.E. Magnetic Pyrochlore Oxides. *Rev. Mod. Phys.* **2010**, *82*, 53. [CrossRef]
4. Hallas, A.M.; Wiebe, C.R. Frustration under pressure: Exotic magnetism in new pyrochlore oxides. *APL Mater.* **2015**, *3*, 041519.
5. Morosan, E.; Fleitman, J.A.; Huang, Q.; Lynn, J.W.; Chen, Y.; Ke, X.; Dahlberg, M.L.; Schiffer, P.; Craley, C.R.; Cava, R.J. Structure and magnetic properties of the $Ho_2Ge_2O_7$ pyrogermanate. *Phys. Rev. B* **2008**, *77*, 224423. [CrossRef]
6. Walker, D.; Carpenter, M.A.; Hitch, C.M. Some simplifications to multianvil devices for high pressure experiment. *Am. Minerol.* **1990**, *75*, 1020–1028.
7. Schmehr, J.L.; Wilson, S.D. Active crystal growth techniques for quantum materials. *Ann. Rev. Mater. Res.* **2017**, *47*, 153–174. [CrossRef]
8. Ross, K.A.; Proffen, T.; Dabkowska, H.A.; Quilliam, J.A.; Yaraskavitch, L.R.; Kycia, J.B.; Gaulin, B.D. Lightly stuffed pyrochlore structure of single-crystalline $Yb_2Ti_2O_7$ grown by the optical floating zone technique. *Phys. Rev. B* **2012**, *86*, 174424. [CrossRef]
9. Kermarrec, E.; Gaudet, D.D.M.J.; Fritsch, K.; Pomaranski, D.; Kycia, J.B.; Qiu, Y.; Copley, J.R.D.; Couchman, M.M.P.; Morningstar, A.O.R.; Dabkowska, H.A.; et al. Gapped and gapless short-range-ordered magnetic states with (1/2, 1/2, 1/2) wave vectors in the pyrochlore magnet $Tb_{2+x}Ti_{2-x}O_{7+\delta}$. *Phys. Rev. B* **2015**, *92*, 245114. [CrossRef]
10. Blanchard, P.E.R.; Clements, R.; Kennedy, B.J.; Ling, C.D.; Reynolds, E.; Avdeev, M.; Stampfl, A.P.J.; Zhang, Z.; Jang, L.Y. Does local disorder occur in the pyrochlore zirconates? *Inorg. Chem.* **2012**, *51*, 13237–13244. [CrossRef] [PubMed]
11. Wiebe, C.R.; Gardner, J.S.; Kim, S.-J.; Luke, G.M.; Wills, A.S.; Greedan, J.E.; Swainson, I.; Qiu, Y.; Jones, C. Magnetic ordering in the spin ice candidate $Ho_2Ru_2O_7$. *Phys. Rev. Lett.* **2004**, *93*, 076403. [CrossRef] [PubMed]
12. Li, X.; Cai, Y.Q.; Cui, Q.; Jin, C.L.; Dun, Z.L.; Matsubayashi, K.; Uwatoko, Y.; Sato, Y.; Kawae, T.; Lv, S.J.; et al. Long-range magnetic order in the Heisenberg pyrochlore antiferromagnets $Gd_2Ge_2O_7$ and $Gd_2Pt_2O_7$ synthesized under high pressure. *Phys. Rev. B* **2016**, *94*, 214429. [CrossRef]
13. Stewart, J.R.; Gardner, J.S.; Qiu, Y.; Ehlers, G. Collective dynamics in the Heisenberg pyrochlore antiferromagnet $Gd_2Sn_2O_7$. *Phys. Rev. B* **2008**, *78*, 132410. [CrossRef]
14. Freitas, R.S.; Gardner, J.S. The magnetic phase diagram of $Gd_2Sn_2O_7$. *J. Phys. Condens. Matter* **2011**, *23*, 164215. [CrossRef]

15. Bonville, P.; Hodges, J.A.; Ocio, M.; Sanchez, J.P.; Vulliet, P.; Sosin, S.; Braithwaite, D. Low temperature magnetic properties of geometrically frustrated $Gd_2Sn_2O_7$. *J. Phys. Condens. Matter* **1003**, *15*, 7777. [CrossRef]
16. Wills, A.S.; Zhitomirsky, M.E.; Canals, B.; Sanchez, J.P.; Bonville, P.; de Reotier, P.D.; Yaouanc, A. Magnetic ordering in $Gd_2Sn_2O_7$: The archetypal Heisenberg pyrochlore antiferromagnet. *J. Phys. Condens. Matter* **2006**, *18*, L37. [CrossRef]
17. Palmer, S.E.; Chalker, J.T. Order induced by dipolar interactions in a geometrically frustrated antiferromagnet. *Phys. Rev. B* **2000**, *62*, 488. [CrossRef]
18. Raju, N.P.; Dion, M.; Gingras, M.J.P.; Mason, T.E.; Greedan, J.E. Transition to long-range magnetic order in the highly frustrated insulating pyrochlore antiferromagnet $Gd_2Ti_2O_7$. *Phys. Rev. B* **1999**, *59*, 14489. [CrossRef]
19. Stewart, J.R.; Ehlers, G.; Wills, A.S.; Bramwell, S.T.; Gardner, J.S. Phase transitions, partial disorder and multi-k structures in $Gd_2Ti_2O_7$. *J. Phys. Condens. Matter* **2004**, *16*, L321. [CrossRef]
20. Paddison, J.A.M.; Cairns, A.B.; Khalyavin, D.D.; Manuel, P.; Daoud-Aladine, A.; Ehlers, G.; Petrenko, O.A.; Gardner, J.S.; Zhou, H.D.; Goodwin, A.L.; et al. Nature of Partial Magnetic Order in the Frustrated Antiferromagnet $Gd_2Ti_2O_7$. Available online: https://arxiv.org/abs/1506.05045 (accessed on 15 February 2019).
21. Sleight, A. New Ternary Oxides of Tetravalent Platinum and Palladium with the Pyrochlore Structure. *Mater. Res. Bull.* **1968**, *3*, 699–704. [CrossRef]
22. Hallas, A.M.; Arevalo-Lopez, A.M.; Sharma, A.Z.; Munsie, T.; Attfield, J.P.; Wiebe, C.R.; Luke, G.M. Magnetic frustration in lead pyrochlores. *Phys. Rev. B* **2015**, *91*, 104417. [CrossRef]
23. Matsuhira, K.; Hinatsu, Y.; Tenya, K.; Sakakihara, T. Low temperature magnetic properties of frustrated pyrochlore ferromagnets $Ho_2Sn_2O_7$ and $Ho_2Ti_2O_7$. *J. Phys. Condens. Matter* **2000**, *12*, 649. [CrossRef]
24. Ehlers, G.; Cornelius, A.L.; Fennell, T.; Koza, M.; Bramwell, S.T.; Gardner, J.S. Evidence for two distinct spin relaxation mechanisms in "hot" spin ice $Ho_2Ti_2O_7$. *J. Phys. Condens. Matter* **2004**, *16*, 635. [CrossRef]
25. Zhou, H.D.; Cheng, J.G.; Hallas, A.M.; Wiebe, C.R.; Li, G.; Balicas, L.; Zhou, J.S.; Goodenough, J.B.; Gardner, J.S.; Choi, E.S. Chemical Pressure Effects on Pyrochlore Spin Ice. *Phys. Rev. Lett.* **2012**, *18*, 207206. [CrossRef] [PubMed]
26. Zhou, H.D.; Bramwell, S.T.; Cheng, J.G.; Wiebe, C.R.; Li, G.; Balicas, L.; Bloxsom, J.A.; Silverstein, H.J.; Zhou, J.S.; Goodenough, J.B.; et al. High pressure route to generate magnetic monopole dimers in spin ice. *Nat. Commun.* **2011**, *2*, 478. [CrossRef] [PubMed]
27. Den Hertog, B.C.; Gingras, M.J.P. Dipolar Interactions and Origin of Spin Ice in Ising Pyrochlore Magnets. *Phys. Rev. Lett.* **2000**, *84*, 3430. [CrossRef]
28. Melko, R.G.; Gingras, M.J.P. Monte Carlo studies of the dipolar spin ice model. *J. Phys. Condens. Matter* **2004**, *16*, R1277. [CrossRef]
29. Hallas, A.M.; Paddison, J.A.M.; Silverstein, H.J.; Goodwin, A.L.; Stewart, J.R.; Wildes, A.R.; Cheng, J.G.; Zhou, J.S.; Goodenough, J.B.; Choi, E.S.; et al. Statics and dynamics of the highly correlated spin ice $Ho_2Ge_2O_7$. *Phys. Rev. B* **2012**, *86*, 134431. [CrossRef]
30. Prando, G.; Carretta, P.; Giblin, S.R.; Lago, J.; Pin, S.; Ghigna, P. Dilution effects in $Ho_{2-x}Y_xSn_2O_7$: From the spin ice to the single-ion magnet. *J. Phys. Conf. Ser.* **2009**, *145*, 012033. [CrossRef]
31. Bramwell, S.T.; Harris, M.J.; den Hertog, B.C.; Gingras, M.J.P.; Gardner, J.S.; McMorrow, D.F.; Wildes, A.R.; Cornelius, A.L.; Champion, J.D.M.; Melko, R.G.; et al. Spin Correlations in $Ho_2Ti_2O_7$: A Dipolar Spin Ice System. *Phys. Rev. Lett.* **2001**, *87*, 047205. [CrossRef] [PubMed]
32. Ramirez, A.P.; Hayashi, A.; Cava, R.J.; Siddharthan, R.; Shastry, B.S. Zero-point entropy in "spin ice". *Nature* **1999**, *399*, 333. [CrossRef]
33. Hallas, A.M.; Cheng, J.G.; Arevalo-Lopez, A.M.; Silverstein, H.J.; Su, Y.; Sarte, P.M.; Zhou, H.D.; Choi, E.S.; Attfield, J.P.; Luke, G.M.; et al. Incipient Ferromagnetism in $Tb_2Ge_2O_7$: Application of Chemical Pressure to the Enigmatic Spin-Liquid Compound $Tb_2Ti_2O_7$. *Phys. Rev. Lett.* **2014**, *113*, 267205. [CrossRef] [PubMed]
34. Gingras, M.J.P.; den Hertog, B.C.; Faucher, M.; Gardner, J.S.; Dunsiger, S.R.; Chang, L.J.; Gaulin, B.D.; Raju, N.P.; Greedan, J.E. Thermodynamic and single-ion properties of Tb^{3+} within the collective paramagnetic-spin liquid state of the frustrated pyrochlore antiferromagnet $Tb_2Ti_2O_7$. *Phys. Rev. B* **2000**, *62*, 6496. [CrossRef]
35. Molavian, H.R.; Gingras, M.J.P.; Canals, B. Dynamically Induced Frustration as a Route to a Quantum Spin Ice State in $Tb_2Ti_2O_7$ via Virtual Crystal Field Excitations and Quantum Many-Body Effects. *Phys. Rev. Lett.* **2007**, *98*, 157204. [CrossRef]

36. Onoda, S.; Tanaka, Y. Quantum Melting of Spin Ice: Emergent Cooperative Quadrupole and Chirality. *Phys. Rev. Lett.* **2010**, *105*, 047201. [CrossRef] [PubMed]
37. Fennell, T.; Kenzelmann, M.; Roessli, B.; Haas, M.K.; Cava, R.J. Power-Law Spin Correlations in the Pyrochlore Antiferromagnet $Tb_2Ti_2O_7$. *Phys. Rev. Lett.* **2012**, *109*, 017201. [CrossRef]
38. Yin, L.; Xia, J.S.; Takano, Y.; Sullivan, N.S.; Li, Q.J.; Sun, X.F. Low-Temperature Low-Field Phases of the Pyrochlore Quantum Magnet $Tb_2Ti_2O_7$. *Phys. Rev. Lett.* **2013**, *110*, 137201. [CrossRef]
39. Fritsch, K.; Ross, K.A.; Qiu, Y.; Copley, J.R.D.; Guidi, T.; Bewley, R.I.; Dabkowska, H.A.; Gaulin, B.D. Antiferromagnetic spin ice correlations at (1/2, 1/2, 1/2) in the ground state of the pyrochlore magnet $Tb_2Ti_2O_7$. *Phys. Rev. B* **2013**, *87*, 094410. [CrossRef]
40. Hallas, A.M.; Gaulin, B.D. Magnetic ordering in the spin liquid candidate $Tb_2Ge_2O_7$. *Phys. Rev. Lett.* Pending Submitted.
41. Hallas, A.M.; Gaudet, J.; Gaulin, B.D. Experimental insights into ground-state selection of quantum XY pyrochlores. *Annu. Rev. Condens. Matter Phys.* **2017**, *9*, 105–124. [CrossRef]
42. Li, X.; Li, W.M.; Matsubayashi, K.; Sato, Y.; Jin, C.Q.; Uwatoko, Y.; Kawae, T.; Hallas, A.M.; Wiebe, C.R.; Arevalo-Lopez, A.M.; et al. Long-range antiferromagnetic order in the frustrated XY pyrochlore antiferromagnet $Er_2Ge_2O_7$. *Phys. Rev. B* **2014**, *89*, 064409. [CrossRef]
43. Dun, Z.L.; Li, X.; Freitas, R.S.; Arrighi, E.; Cruz, C.R.D.; Lee, M.; Choi, E.S.; Cao, H.B.; Silverstein, H.J.; Wiebe, C.R.; et al. Antiferromagnetic order in the pyrochlores $R_2Ge_2O_7$ (R = Er, Yb). *Phys. Rev. B* **2015**, *92*, 140407. [CrossRef]
44. Champion, J.D.M.; Harris, M.J.; Holdsworth, P.C.W.; Wills, A.S.; Balakrishnan, G.; Bramwell, S.T.; Cizmar, E.; Fennell, T.; Gardner, J.S.; Lago, J.; et al. $Er_2Ti_2O_7$: Evidence of quantum order by disorder in a frustrated antiferromagnet. *Phys. Rev. B* **2003**, *68*, 020401(R). [CrossRef]
45. Poole, A.; Wills, A.S.; Lelievre-Berna, E. Magnetic ordering in the XY pyrochlore antiferromagnet $Er_2Ti_2O_7$ a spherical neutron polarimetry study. *J. Phys. Condens. Matter* **2007**, *19*, 452201. [CrossRef]
46. Dun, Z.L.; Lee, M.; Choi, E.S.; Hallas, A.M.; Wiebe, C.R.; Gardner, J.S.; Arrighi, E.; Freitas, R.S.; Arevalo-Lopez, A.M.; Attfield, J.P.; et al. Chemical pressure effects on magnetism in the quantum spin liquid candidates $Yb_2X_2O_7$ (X = Sn, Ti, Ge). *Phys. Rev. B* **2014**, *89*, 064401. [CrossRef]
47. Hallas, A.M.; Gaudet, J.; Wilson, M.N.; Munsie, T.J.; Aczel, A.A.; Stone, M.B.; Freitas, R.S.; Arevalo-Lopez, A.M.; Attfield, J.P.; Tachibana, M.; et al. Antiferromagnetic ground state in the effective S = 1/2 pyrochlore $Yb_2Ge_2O_7$. *Phys. Rev. B* **2016**, *93*, 104405. [CrossRef]
48. Guitteny, S.; Petit, S.; Lhotel, E.; Robert, J.; Bonville, P.; Forget, A.; Mirebeau, I. Palmer-Chalker correlations in the XY pyrochlore antiferromagnet $Er_2Sn_2O_7$. *Phys. Rev. B* **2013**, *88*, 134408. [CrossRef]
49. Petit, S.; Lhotel, E.; Damay, F.; Boutrouille, P.; Forget, A.; Colson, D. Long range order in the dipolar XY antiferromagnet $Er_2Sn_2O_7$. *Phys. Rev. Lett.* **2017**, *119*, 187202. [CrossRef]
50. De Reotier, P.D.; Yaouanc, A.; Chapuis, Y.; Curnoe, S.H.; Grenier, B.; Ressouche, E.; Marin, C.; Lago, J.; Baines, C.; Giblin, S.R. Magnetic order, magnetic correlations, and spin dynamics in the pyrochlore antiferromagnet $Er_2Ti_2O_7$. *Phys. Rev. B* **2012**, *86*, 104424. [CrossRef]
51. Yaouanc, A.; de Reotier, P.D.; Bonville, P.; Hodges, J.A.; Glazkov, V.; Keller, L.; Sikolenko, V.; Bartkowiak, M.; Amato, A.; Baines, C.; et al. Dynamical Splayed Ferromagnetic Ground State in the Quantum Spin Ice $Yb_2Sn_2O_7$. *Phys. Rev. Lett.* **2013**, *110*, 127207. [CrossRef]
52. Hodges, J.A.; Bonville, P.; Forget, A.; Yaouanc, A.; de Reotier, P.D.; Andre, G.; Rams, M.; Krolas, K.; Ritter, C.; Gubbens, P.C.M.; et al. First Order Transition in the Spin Dynamics of Geometrically Frustrated $Yb_2Ti_2O_7$. *Phys. Rev. Lett.* **2002**, *88*, 077204. [CrossRef]
53. Chang, L.J.; Onoda, S.; Su, Y.; Kao, Y.J.; Tsuei, K.D.; Yasui, Y.; Kakurai, K.; Lees, M.R. Higgs transition from a magnetic Coulomb liquid to a ferromagnet in $Yb_2Ti_2O_7$. *Nat. Commun.* **2012**, *3*, 992. [CrossRef] [PubMed]
54. Savary, L.; Balents, L. Disorder-Induced Entanglement in Spin Ice Pyrochlores. *Phys. Rev. Lett.* **2012**, *108*, 037202. [CrossRef] [PubMed]
55. Wong, A.W.C.; Hao, Z.; Gingras, M.J.P. Ground State Phase Diagram of Generic XY Pyrochlore Magnets with Quantum Fluctuations. *Phys. Rev. B* **2013**, *88*, 144402. [CrossRef]
56. Hallas, A.M.; Gaudet, J.; Butch, N.P.; Tachibana, M.; Freitas, R.S.; Luke, G.M.; Wiebe, C.R.; Gaulin, B.D. Universal Dynamic Magnetism in Yb-Pyrochlores with Disparate Ground States. *Phys. Rev. B* **2016**, *93*, 100403. [CrossRef]

57. Stoter, T.; Antlauf, M.; Opherden, L.; Gottschall, T.; Honung, J.; Gronemann, J.; Herrmannsdorfer, T.; Granovsky, S.; Schwartz, M.; Doerr, M.; et al. Tuning Interactions in the Spin-Ice Materials $Dy_2Ge_{2-x}Si_xO_7$ by Silicon Substitution. Available online: https://arxiv.org/abs/1809.01480 (accessed on 15 February 2019).
58. Hallas, A.M.; Sharma, A.Z.; Mauws, C.; Chen, Q.; Zhou, H.D.; Ding, C.; Gong, Z.; Tachibana, M.; Sarte, P.M.; Attfield, J.P.; et al. Coexistence of metallic and nonmetallic properties in the pyrochlore $Lu_2Rh_2O_7$. *NPJ Quantum Mater.* **2019**, *4*, 9. [CrossRef]
59. Hallas, A.M.; Sharma, A.Z.; Cai, Y.; Munsie, T.J.; Wilson, M.N.; Tachibana, M.; Wiebe, C.R.; Luke, G.M. Relief of Frustration in the Heisenberg Pyrochlore Antiferromagnet $Gd_2Pt_2O_7$. *Phys. Rev. B* **2016**, *94*, 134417. [CrossRef]
60. Hallas, A.M.; Gaudet, J.; Butch, N.P.; Xu, G.Y.; Tachibana, M.; Wiebe, C.R.; Luke, G.M.; Gaulin, B.D. Phase Competition in the Palmer-Chalker XY Pyrochlore $Er_2Pt_2O_7$. *Phys. Rev. Lett.* **2017**, *119*, 187201. [CrossRef]
61. Cai, Y.Q.; Jiao, Y.Y.; Cui, Q.; Li, Y.; Wang, B.S.; Fernandez-Diaz, M.T.; McGuire, M.A.; Yan, J.-Q.; Alonso, J.A.; Cheng, J.-G. Giant reversible magnetocaloric effect in the pyrochlore $Er_2Mn_2O_7$ due to a cooperative two-sublattice ferromagnetic order. *Phys. Rev. Mater.* **2017**, *6*, 064408. [CrossRef]
62. Klein, R.A.; Walsh, J.P.S.; Clarke, S.M.; Guo, Y.S.; Bi, W.L.; Fabbris, G.; Meng, Y.; Haskel, D.; Alp, E.E.; van Duyne, R.P.; et al. Impact of magnetic order in Jarosite. *J. Am. Chem. Soc.* **2018**, *140*, 12001–12009. [CrossRef]
63. Somayazulu, M.; Ahart, M.; Mishra, A.K.; Geballe, Z.M.; Baldini, M.; Meng, Y.; Struzhkin, V.V.; Hemley, R.J. Evidence for Superconductivity above 260 K in Lanthanum Superhydride at Megabar Pressures. *Phys. Rev. Lett.* **2019**, *122*, 027001. [CrossRef] [PubMed]
64. Greedan, J.E.; Gout, D.; Lozano-Gorrin, A.D.; Derahkshan, S.; Proffen, T.; Kim, H.-J.; Bozin, E.; Billinge, S.J.L. Local and average structures of the spin-glass pyrochlore $Y_2Mo_2O_7$ from neutron diffraction and neutron pair distribution function analysis. *Phys. Rev. B* **2009**, *79*, 014427. [CrossRef]